J. Plasma Phys. (2023), *vol*. 89, 905890209
Published by Cambridge University Press

doi:10.1017/S0022377823000247

Laser wakefield acceleration of electrons using Bessel–Gauss doughnut beams for accelerating beam guiding

V. Tomkus[1,†], **V. Girdauskas**[1,2], **M. Abedi-Varaki**[1] **and G. Raciukaitis**[1]

[1]Center for Physical Sciences and Technology, Savanorių 231, 02300 Vilnius, Lithuania

[2]Vytautas Magnus University, K. Donelaicio st.58, LT-44248 Kaunas, Lithuania

(Received 4 December 2022; revised 4 March 2023; accepted 6 March 2023)

A high-intensity laser pulse propagating through a gas target disturbs the uniform plasma distribution. Plasma density structures, created by high-order Bessel–Gauss beams for guiding the accelerating Gaussian beam and laser wakefield acceleration of electrons, are analysed using Wake-T and Fourier–Bessel particle-in-cell (FBPIC) simulation tools. The use of Bessel–Gauss doughnut beams increases the acceleration distance and energy of accelerated electrons up to 2.3 times at a 2 mm distance relative to the Gaussian beam of the same intensity.

Key words: plasma simulation, plasma applications, plasma waves

1. Introduction

Laser–plasma interaction of high-peak-power femtosecond (fs) and kilohertz-class lasers with a wide range of applications is an exciting area of research (Malka *et al.* 2008; Rovige *et al.* 2020; Hidding *et al.* 2023). The propagation of the laser pulses over a long distance and the ability to create a plasma channel and control its length are significant subjects of research on laser wakefield accelerators (LWFAs) (Andreev *et al.* 1998; Tomassini *et al.* 2018; Palastro *et al.* 2020). The energy of accelerated electrons depends on the laser–plasma interaction length (which is proportional to the Rayleigh length). The investigated methods of increasing laser–plasma interaction length and accelerating beam guiding can be divided into three categories: (1) self-focused propagation; (2) propagation in hollow fibre structures; and (3) laser-pulse pre-formed plasma waveguides. The first method is associated with relativistic self-focusing and ponderomotive charge displacement by the femtosecond laser pulse. By employing this method, the refractive index of the on-axis plasma channel increases with the relativistic increase of electron inertia near the centre of the beam and ponderomotive charge expulsion to the side of the channel (Milchberg *et al.* 2006). Self-focusing of the laser pulse in an ionised gas facilitates the guiding of the laser pulse beyond its Rayleigh length. However, the process typically depends delicately on plasma instabilities (Esarey, Schroeder & Leemans 2009).

† Email address for correspondence: vidmantas.tomkus@ftmc.lt

Implementation of the second method allows to produce a stable plasma-guiding channel and accelerate electron bunches up to 8 GeV. This technique was realised by propagating of the accelerating laser pulse in a capillary with a gas pre-ionised by discharge current and preheated with a supplementary laser pulse. It led to the creation of a parabolic plasma channel guiding the accelerating high-peak-power laser pulse over approximately 10 cm (Leemans *et al.* 2014; Gonsalves *et al.* 2019). The third method was implemented using an axicon lens or parabolic mirror with extended focal depth to pre-ionise the gas along the extended focal area and produce the guiding plasma channel. A parabolic plasma channel was formed within a few nanoseconds due to the hydrodynamic expansion of pre-ionised plasma. Experimental and theoretical investigations have demonstrated that the recombination process and the lifetime of a plasma channel created by a single femtosecond laser pulse was in the range of several nanoseconds (Tzortzakis *et al.* 2000). A long pre-ionising laser pulse allows to heat the plasma electrons by inverse Bremsstrahlung and increase the channel lifetime (Hao *et al.* 2005). However, long pulses, due to diffraction losses, are challenging to propagate over long distances and it is difficult to cope with the guiding requirements of using such a guiding scheme. Another way to form the parabolic plasma channel is to use the relativistic and ponderomotive self-channelling of the pre-ionising laser pulse (Mohamed *et al.* 2011). Recently, the laser-pulse pre-formed plasma guiding channels produced using various techniques have been studied by several authors (Osterhoff *et al.* 2008; Zhang *et al.* 2016; Smartsev *et al.* 2019; Chitgar *et al.* 2020; Tang *et al.* 2020). Lu *et al.* (2015) considered a quasi-steady-state plasma channel with a 60–80 ns lifetime formed by pulse sequences of a femtosecond laser in air. Smartsev *et al.* (2019) presented the axiparabola as a novel reflective optics instrument that permits prolonging the propagation of diffraction-free high-peak-power and broadband laser pulses. It was observed that a laser beam shaped by axiparabola forms a 10 mm long plasma channel and guides a 20 TW laser radiation over nearly 10 Rayleigh lengths. Shalloo *et al.* (2018) showed that fully ionised and low-density plasma channels could be produced by the hydrodynamic expansion of plasma columns generated by optical field ionisation (OFI). Furthermore, it was found that an axicon lens could be used to generate long plasma channels with on-axis densities of the order of $n_e \approx 10^{17}$ cm^{-3}, matched spot-sizes $w_M \approx 40$ μm, and attenuation lengths of the order of $L_{\text{att}} \sim 1000$ mm. Lemos *et al.* (2018) explored the plasma waveguides produced by the laser pulses with intensities of $\sim 10^{15}$ W cm^{-2} in an 8 mm long hydrogen plasma waveguide with a 35 % guiding efficiency. Zhang *et al.* (2016) investigated the electron beam acceleration with multiple transverse plasma density structures in a wakefield driven by a Laguerre–Gauss (LG) pulse through three-dimensional particle-in-cell (PIC) simulations. It was found that the wakefield has various transverse structures under proper conditions, and it was demonstrated that the doughnut-like wakefield structures could accelerate the ring-shaped hollow electron beam. Tang *et al.* (2020) studied the propagation dynamics of the azimuthally polarised first-order Bessel–Gauss (BG) laser beam in a parabolic plasma channel by using a two-dimensional PIC simulation. It was observed that the evolution of this dark hollow laser beam during propagation in the plasma channel could be classified into three types: (1) the propagation with a constant ring-shaped beam radius and width; (2) the synchronous periodic defocusing oscillation; (3) the synchronous periodic focusing oscillation. Vieira & Mendonça (2014) considered the nonlinear laser-driven doughnut wakefield for positron and electron acceleration. The authors have shown that nonlinear wakefield driven by LG laser pulses can lead to the self-injection of a ring-shaped electron bunch and positron acceleration. The high-order modes of the laser beam form a doughnut-shaped wakefield able to accelerate positrons similarly as electrons are accelerated in a spherical bubble.

https://doi.org/10.1017/S0022377823000247 Published online by Cambridge University Press

This paper aims to study the effects of LWFA accelerating pulse guiding of a doughnut Bessel–Gauss beam by using the PIC simulation method. The research is pushed by the progress in high-intensity, high-repetition-rate OPCPA lasers (Budriūnas *et al.* 2017), which seem to be a promising alternative for LWFA applications to 10 Hz Ti:sapphire lasers with >30 fs pulse durations and a few Joule pulse energies. The emerging kHz-class lasers typically operate at a lower pulse energy of tens of millijoules and have a pulse duration of 7–10 fs. To drive the charged particles using this type of laser in the LWFA self-guiding bubble regime, plasma concentrations of $n = 3\text{–}5 \times 10^{19}$ cm^{-3} are required (Faure *et al.* 2018). Consequently, the diameter of the plasma bubble reduces from the typical 25 μm to 8 μm and tighter focusing of the laser beam is required. It leads to shorter acceleration distances of hundreds of micrometres, relatively low energy and high energy spread of accelerated electrons. Lowering the plasma concentration down to $n = 3 \times 10^{18}$ cm^{-3} would increase the acceleration distance. However, the available laser pulse energy of 40–60 mJ focused to the laser beam waist of 7–8 μm only allows reaching the intensities with the laser strength parameter $a_0 = 1.5\text{–}2$. The laser beam propagation is no longer in a self-guiding regime and additional means for extending acceleration distance are required. The increase of the acceleration distance with the laser-beam guiding permits getting electron bunches with higher energy, lower energy spread and divergence required by various potential applications such as compact secondary X-ray sources and very high energy electron (VHEE) radiotherapy (Fuchs *et al.* 2009; Subiel *et al.* 2017; Kokurewicz *et al.* 2019).

The parameters and stability of accelerated electrons depend also on the proper position and duration of electron injection into the plasma wakefield. Generally, to define the position of injection and control the charge of accelerated electrons, different approaches of injection as density down-ramp triggered injection (Gonsalves *et al.* 2011; Burza *et al.* 2013; Hansson *et al.* 2015; Massimo *et al.* 2017; Cardenas *et al.* 2020), injection by a second laser beam (Fubiani *et al.* 2004; Brijesh *et al.* 2012), ionisation-assisted (Golovin *et al.* 2016) or self-truncated electron injection (Mirzaie *et al.* 2015) are used. In the down-ramp density triggered injection cases, the formation of sharp plasma concentration gradients by using two nozzles (Gonsalves *et al.* 2011), and insertion of a wire (Burza *et al.* 2013), razor blade (Cardenas *et al.* 2020) or capillary jet (Hansson *et al.* 2015) into the nozzle jet causing shock waves have been implemented. An alternative approach for better control of the injection with the position having a precision of 20–40 μm was proposed by manufacturing one-sided shock (OSS) nozzle from single block of fused silica using the three-dimensional (3-D) laser machining technique (Rovige *et al.* 2020). The precise control of injection position by two beams was realized by Brijesh *et al.* (2012) and Fubiani *et al.* (2004). An ionization injection scheme, using the combination of two nozzles injecting nitrogen mixed into the light gases, such as He or H_2, and a second section with pure He or H_2, was investigated by Golovin *et al.* (2016).

Advances in free-shape optics manufacturing permit getting nearly any desired spatial-temporal distribution of laser energy. We performed detailed simulations of the laser–plasma interaction using combined Bessel–Gauss doughnut-shaped and Gaussian laser pulses with a delay between laser pulses at a femtosecond scale. In this article, we investigate plasma structures excited by the Bessel–Gauss doughnut beam for guiding the accelerating Gaussian beam and laser wakefield acceleration of electrons using the Wake-T and FBPIC simulation tools.

2. Methods

Two open-source PIC simulation tools, Wake-T (Pousa, Aßmann & de la Ossa 2019) and FBPIC (Lehe *et al.* 2016), were used for numerical simulation. The 3-D code Wake-T

https://doi.org/10.1017/S0022377823000247 Published online by Cambridge University Press

uses two-dimensional (2-D) cylindrical geometry (r,z) and quasi-static approximation (Pukhov 2015). The laser pulse evolution was modelled by solving the equation of the vector potential of the envelope (Benedetti *et al.* 2017) rather than simulating the laser wave field. Therefore, it was not necessary to comply with the strict limitation on the simulation step size of the temporal coordinate resulting from the Courant condition. The step size was not limited by the laser wavelength scale; the limitation was only due to the plasma wavelength and Rayleigh length, which are much larger than the laser wavelength. Therefore, the computational efficiency of a quasi-static code can be up to six orders of magnitude higher than a standard 3-D PIC code (Pousa *et al.* 2019). When simulating beam guiding with Wake-T, the limitation in BG pulse description is that the 2-D cylindrical geometry does not allow the introduction of the spiral phase of a high-order BG beam. Therefore, in this work, the results presented by Wake-T are obtained when the BG pulse profile fits the amplitude of the envelope function without the helical phase and propagates without modifications due to diffraction or interaction with the plasma.

The assumption that the BG pulse propagates while maintaining a constant spatial and temporal profile is only valid for a certain propagation distance. Therefore, the quasi-3-D FBPIC code, which uses a cylindrical geometry with azimuthal modal decomposition to describe fully the spatial-temporal evolution of the laser beam, was further used to simulate the evolution of the BG pulse and the influence of that evolution on particle acceleration. For the near-cylindrical geometry, only several azimuthal modes are sufficient for beam simulation, making the quasi-3-D code much faster than the standard 3-D PIC code. The performed test simulation results show that including 3 to 5 azimuthal modes are sufficient to model the first- and second-order BG beams with a spiral phase.

The simulations were performed for various amplitudes and durations of the Gaussian and BG pulses, both pulses together, separately for Gaussian and separately for BG pulses. Both pulses had a Gaussian temporal envelope. The size of the coordinate window moving at the speed of light c, $r \times z = 180 \times 60\ \mu\text{m}^2$, was chosen such that in the beam propagation direction (z-axis), it covered both laser pulses and at least two periods of the plasma wave, and along the orthogonal r-coordinate, it was 20/25 times wider than the width of the first ring of the doughnut BG beam. Open-type boundary conditions at the edges of the coordinate window were used to avoid artificial reflection. The number of nodes in the coordinate grid was 600×1200. The number of macroparticles per cell for the Gaussian and the first-order BG beams was (3,3,4), and the number of azimuthal modes was $m = 3$. The number of macroparticles for the second-order Bessel beams was (4,4,5) and the number of azimuthal modes $m = 5$. The number of macroparticles per cell in Wake-T simulations was 5. The width of the Gaussian envelope of the BG beam was 50 times the width of the BG first ring. To avoid interference of Gaussian and BG laser pulses, polarisations of the pulses were set orthogonal. The initial random distribution of particle coordinates and momentum in an injected electron bunch was Gaussian, the transverse and longitudinal RMS length was (1 μm, 1 μm), the charge 1 pC, initial energy 10 MeV, relative energy spread 5 % and the number of bunch macro-particles 10^3.

The Wake-T code was used to simulate the plasma structures formed by the BG beam and the Gaussian pulse guiding properties in the BG plasma wake. The FBPIC code was used to model the electron bunch acceleration by the Gaussian pulse and Gaussian pulse guided in the BG plasma wake.

Laser beam/pulse configurations used in the research were:

(1) Gaussian beam (G);
(2) Bessel–Gauss beam (BG) – doughnut-shaped, first- or second-order optical vortex;
(3) The first-order Bessel–Gauss beam (pulse), followed by a Gauss pulse ($G + B_1G$);

https://doi.org/10.1017/S0022377823000247 Published online by Cambridge University Press

(4) The second-order Bessel–Gauss beam (pulse), followed by a Gauss pulse ($G + B_2G$).

The Gaussian or Bessel–Gauss beam or pulse in the article means transversal energy distribution in the laser pulse, while the temporal shape of the pulse is assumed to be Gaussian.

A 2-D cylindrical quasi-static PIC code Wake-T (Pousa *et al.* 2019) was used to simulate the accelerating laser pulse propagation in a plasma channel generated by a Bessel–Gauss beam. The envelope of the normalised vector potential of the linear-polarised *n*th-order BG beam had the shape:

$$a_b(r, \varphi, \eta) = a_{ob} J_n\left(\frac{r_n}{w_b} r\right) \exp\left(-\frac{r^2}{w_{0b}^2} - \left(\frac{\eta}{c\tau_b}\right)^2 + in\varphi\right), \tag{2.1}$$

where

$$a_{0b} = \frac{eA_b}{m_e c^2}, \tag{2.2}$$

is the amplitude of the normalised vector potential, also called the laser strength parameter; J_n is the *n*th-order Bessel function ($n = 1, 2$); w_b is the distance from the axis of the Bessel beam to the first ring, and for $n = 1$, the constant is $r_n = 1.84$ and for $n = 2$, $r_n = 3$; w_{0b} is the Gaussian envelope radius of the BG beam; $\eta = z - ct - z_{cb}$ is the longitudinal coordinate in the moving coordinate window; z_{cb} is the pulse peak coordinate; τ_b is the pulse duration of the BG beam; r, φ is the radial, azimuthal coordinate. In the Wake-T modelling of the BG beam propagation in plasma, it was assumed that there is no dependency on the azimuthal coordinate, and the envelope of the vector potential is preserved.

The accelerating pulse envelope of the normalised vector potential with the linear polarisation, orthogonal to the polarisation of the BG beam, has the Gaussian temporal and spatial shape:

$$a(r, \eta) = a_o \exp\left(-\frac{r^2}{w_0^2} - \left(\frac{\eta}{c\tau_b}\right)^2\right). \tag{2.3}$$

Here, a_0 is the amplitude of the normalised vector potential, also called the laser strength parameter; w_0 is the radius of the beam; $\eta = z - ct - z_c$ is the longitudinal coordinate in the moving coordinate window; z_c is the pulse peak coordinates; and τ is the pulse duration.

3. Accelerating beam guiding using a high-order Bessel–Gauss beam

3.1. *Dynamic plasma channel for guiding the accelerating beam*

The simulation was performed using the first- and second-order Bessel–Gauss (B_1G and B_2G) beams to understand the influence of the transverse laser beam intensity profile on plasma density distribution, and optical and electron beam guiding. Wake-T simulation results in figure 1 show that when a high-intensity ($a_{0b} > 1$) B_1G beam propagates in a sub-critical concentration plasma, ring-shaped, high electron concentration zones are formed in the plasma, and they are moving together with the plasma wave.

The transverse charge density profiles of the plasma are shown in figure 2. The difference in charge density on the z-axis and at the plasma ring highly depends on the laser beam strength parameter a_0. For higher intensity BG pulse, we would expect a more remarkable effect of the plasma ring on the accelerating laser pulse and electron bunch propagation.

https://doi.org/10.1017/S0022377823000247 Published online by Cambridge University Press

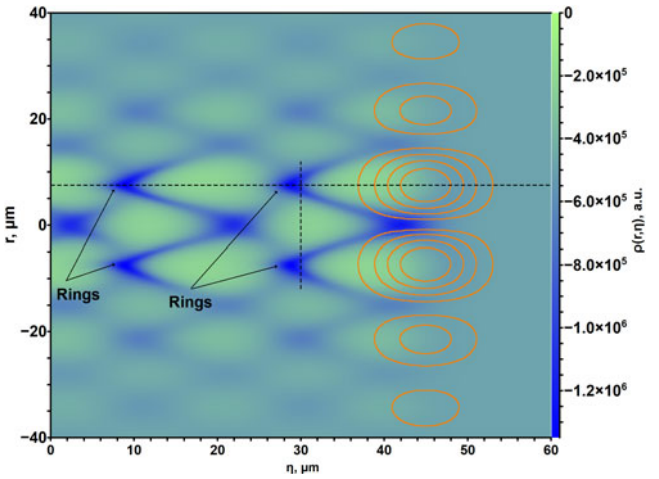

FIGURE 1. Electron charge density distribution $\rho(r,\eta)$ in a B_1G created plasma wave (green-blue) and the first-order B_1G pulse envelope (isolines). Dotted lines mark the positions of longitudinal and transverse cross-sections of charge density profiles shown in figures 2 and 3. Plasma electron concentration $n_0 = 3 \times 10^{18}$ cm^{-3}. B_1G pulse parameters, $a_{0b} = 1.5$; $\tau_b = 25$ fs; $w_{0b} = 7.5$ μm. The laser pulse propagates from the left to right side along the z-axis, centred at $r = 0$.

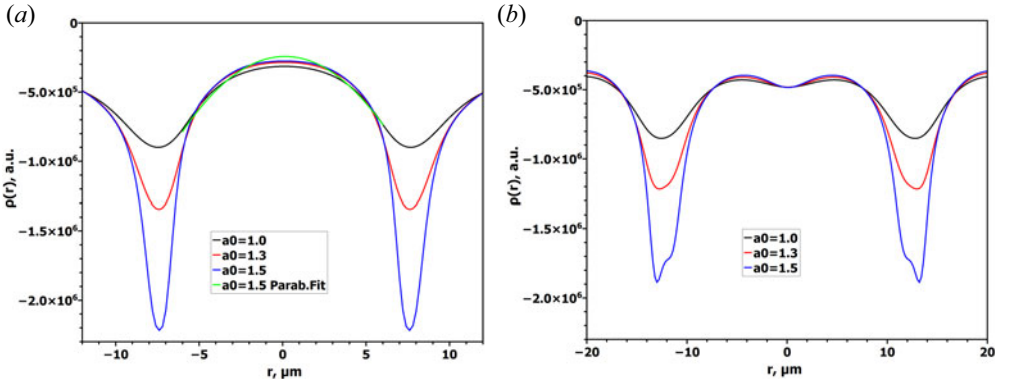

FIGURE 2. Transverse profiles of electron charge density $\rho(r)$ for (a) first-order B_1G and (b) second-order B_2G pulses and various values of the laser strength parameter a_{0b}. The green line in panel (a) is a parabolic approximation. Plasma electron concentration $n_0 = 3 \times 10^{18}$ cm^{-3}. BG pulse parameters, $\tau_b = 25$ fs; $w_{0b} = 7.5$ μm for B_1G and $w_{0b} = 11$ μm for B_2G.

The transverse charge density distribution, presented in figure 2, shows that the charge density profile for the first-order Bessel–Gauss beam (B_1G) near the beam propagation axis at a selected point on the z-axis is close to parabolic (figure 2a). The whole structure moves at the laser group velocity. Therefore, we can expect that the ring-shaped electron concentration distribution moving with the plasma wave will act as a plasma channel (Leemans *et al.* 2014; Gonsalves *et al.* 2019) for guiding the accelerating laser pulse, maintaining its high peak intensity and accelerating injected electron bunch. The transverse profile of the plasma distribution produced by the second-order Bessel–Gauss beam (B_2G) differs significantly from parabolic (figure 2b). However, even with that

https://doi.org/10.1017/S0022377823000247 Published online by Cambridge University Press

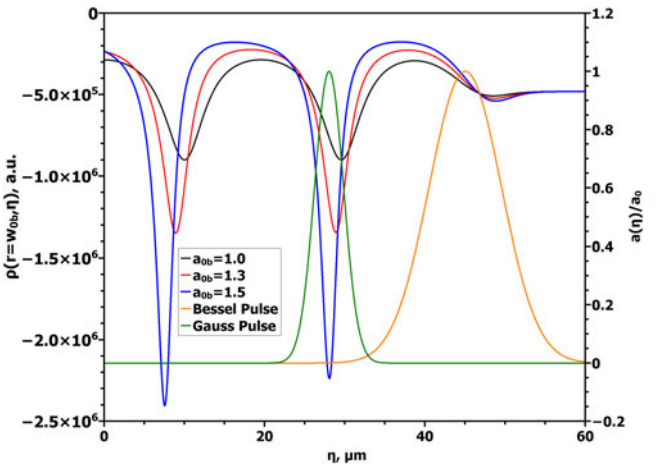

FIGURE 3. Longitudinal profiles of the electron charge density $\rho(\eta)$ for various laser strength parameter values a_{0b} of the B_1G pulse (solid lines) and normalised envelopes of the accelerating Gaussian (green) and B_1G pulses (yellow) (dotted lines). Plasma electron concentration $n_0 = 3 \times 10^{18}$ cm^{-3}. Gaussian pulse duration $\tau = 10$ fs. B_1G pulse parameters, $\tau_b = 25$ fs; $w_{0b} = 7.5$ μm.

plasma density profile, we observe a guiding effect (figure 6*b*). If the laser strength parameter a_{0b} increases from 1 to 1.5, the maximum negative charge density in the ring increases from 3 to more than 7 times relative to the initial plasma density, facilitating better waveguiding properties of the ring-shaped plasma structure.

This waveguide exists only for a limited distance along the beam propagation direction and we performed a detailed simulation of the guiding effect of the plasma electrons ring on the Gaussian laser pulse. The longitudinal charge density profiles of figure 3, along the dotted line shown in figure 1, show that the axial length of the annular high electron concentration zone is approximately 6 μm, which decreases slightly with the increasing a_{0b} parameter of the B_1G beam.

To ensure the waveguiding effect of the plasma channel over the entire length of the accelerating laser pulse (green dotted line in figure 3), the accelerating pulse should fit inside the high-concentration electron ring (dip). Its spatial spread along the propagation direction should be short enough to avoid diffraction losses of energy on the tails of the pulse. In addition, as the group velocity of the BG pulse differs from the accelerating Gaussian pulse, the spatial duration of the accelerating pulse should be less than the axial length of the electron ring. Therefore, a 10 fs long Gaussian pulse was used to drive the acceleration, while the guiding BG pulse was selected to be 25 fs long. Technically that could be implemented by transmitting part of the Gaussian beam with a pulse duration of 10 fs through a transparent phase mask, which not only transforms the beam to Bessel–Gauss, but also extends its duration due to dispersion in bulk.

The Wake-T simulation results also showed that the maximum density of the negative charge in the electron ring depends on the BG pulse duration and the initial plasma electron concentration (figure 4).

With decreasing plasma concentration, the maximum charge density value in the ring 'waveguide cladding' is reached for longer BG pulse durations. For $a_{0b} = 1.5$, the optimal pulse duration of the BG beam forming the parabolic guiding channel increases from 25 fs to 55 fs, decreasing the initial plasma concentration from 3×10^{18} cm^{-3} to $n_0 = 1 \times 10^{18}$ cm^{-3}. A particularly strong dependence of the induced charge density on the

https://doi.org/10.1017/S0022377823000247 Published online by Cambridge University Press

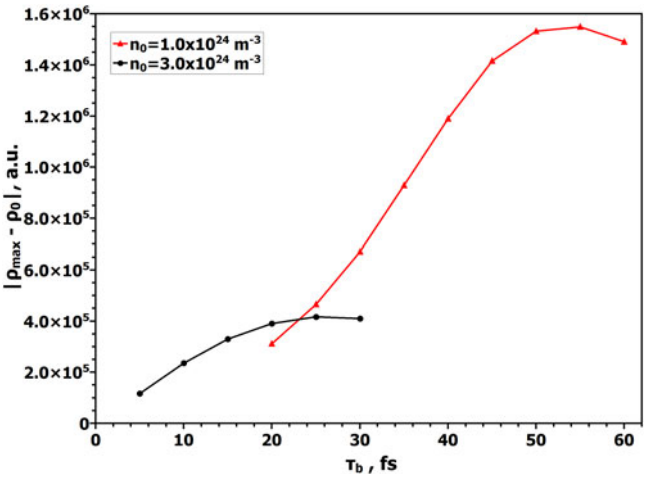

FIGURE 4. Dependence of the difference of maximum charge density $\rho_{\max}$ and initial charge density ρ_0 in the ring-shaped electron plasma wave created by the B_1G laser pulse on its duration for two different initial plasma electron concentrations, $n_0 = 1 \times 10^{18}$ cm^{-3}; $n_0 = 3 \times 10^{18}$ cm^{-3}. B_1G pulse parameters, $a_{0b} = 1.5$; $\tau_b = 25$ fs; $w_{0b} = 7.5$ μm.

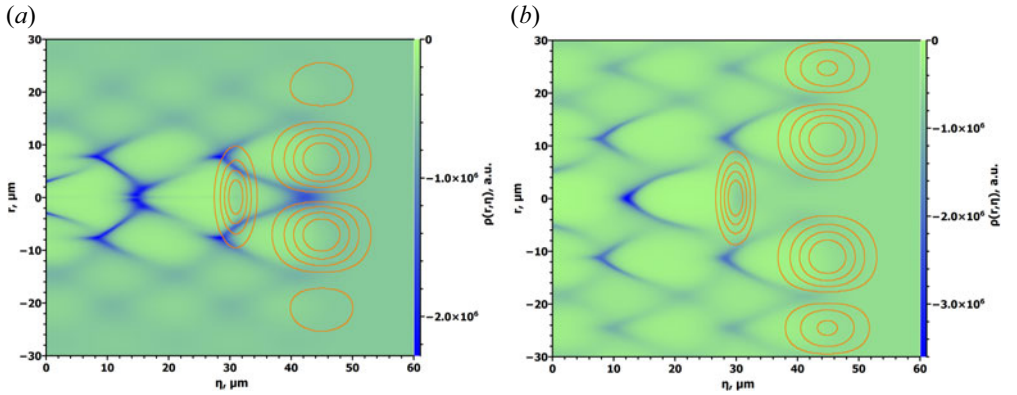

FIGURE 5. Electron charge density distribution $\rho(r,\eta)$ in the plasma wave (green-blue) and the envelopes (isolines) of the accelerating Gaussian pulse and pulses of (*a*) B_1G and (*b*) B_2G beams. Parameters of the accelerating Gaussian beam, $a_0 = 2.0$; $\tau = 10$ fs; $w_0 = 7$ μm; and BG beam, $a_{0b} = 1.5$; $\tau_b = 25$ fs. The waist of B_1G is $w_{0b} = 7.5$ μm in panel (*a*) and the waist of B_2G is $w_{0b} = 11$ μm in panel (*b*).

BG pulse duration is observed for lower plasma concentrations. However, to maintain the lower pulse energy required to reach $a_{0b} = 1.5$, a 25 fs pulse duration for the guiding BG pulses in further simulations was selected.

3.2. *Guiding the accelerating Gaussian beam by the plasma ring*

Simulating the accelerating pulse propagation in the plasma perturbed by the BG pulse, the initial value of the pulse peak coordinate z_c was adjusted to the first dip in the longitudinal charge density profile, corresponding to the high-concentration electron plasma ring (figure 2), and the spatial pulse duration was selected to equal to $c\tau = 3$ μm to fit within the dip in the charge density profile (figure 5).

https://doi.org/10.1017/S0022377823000247 Published online by Cambridge University Press

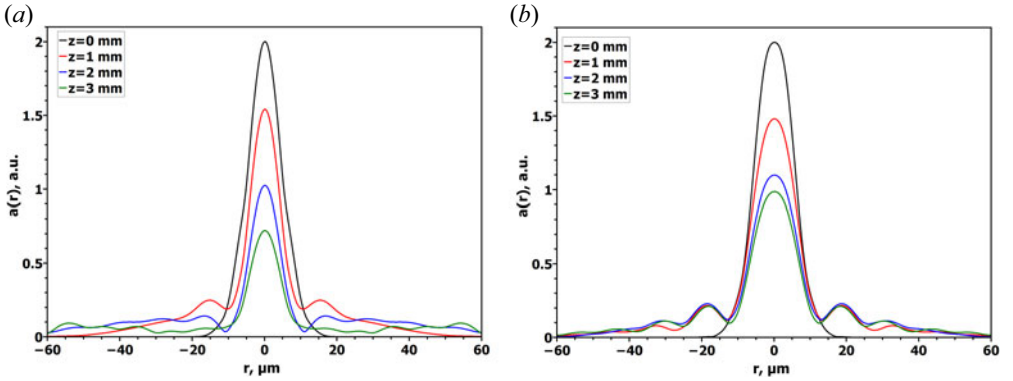

FIGURE 6. Transverse profiles $a(r)$ of the accelerating beam amplitude at the pulse peak, guided by the (*a*) first-order B_1G and (*b*) second-order B_2G beam at various propagation distances in plasma ($z = 0$, 1, 2, 3 mm). Parameters of the accelerating Gaussian beam, $a_0 = 2.0$; $\tau = 10$ fs; $w_0 = 7$ μm; and BG beam, $a_{0b} = 1.5$; $\tau_b = 25$ fs. The waist of B_1G is $w_{0b} = 7.5$ μm and the waist of B_2G is $w_{0b} = 11$ μm.

The simulation results show that the guiding effect on the propagation of the accelerating pulse in the BG pulse plasma wake is evident as the central part of the accelerating beam maintains an almost constant diameter at a distance of ten and more times the Rayleigh length of the beam $z_R = \pi w_0^2/\lambda$ (figure 6).

However, the maximum amplitude of the accelerating beam decreases with the propagation distance due to the leak of laser energy through the 'soft waveguide cladding' and the difference in the group velocity of the accelerating pulse from the group velocity of the BG pulse. At the initial propagation distance (<0.4 mm), the guiding profile of the moving plasma waveguide is formed, which depends on the ratio of the initial radius of the accelerating beam to the radius of the doughnut BG beam. When the propagation distance exceeds $\sim 10 z_R$, the modulation of the temporal envelope of the pulse begins to become apparent. For the distance exceeding $\sim 20 z_R$ ($\sim$3.7 mm), the laser pulse is decomposed into several pulses separated in time, and the maximum laser intensity falls significantly. Therefore, we have a limited acceleration distance less than 3 mm.

4. Electron acceleration using a higher-order Bessel–Gauss beam

Based on the initial simulation results of 2-D quasi-static PIC code Wake-T, the more advanced FBPIC code was used to model laser wakefield acceleration of electrons using higher-order Bessel–Gauss beams. B_1G and B_2G cases were modelled. As a probe, a Gaussian electron bunch with a charge of 1 pC, a standard deviation of $\sigma_{r,z} = 1$ μm in longitudinal and transversal direction, a relative electron energy spread of 5 %, and initial energy of 10 MeV was injected at the position of the maximum of the longitudinal electric field E_z of the plasma wave. The selected parameters of the injected charge allow for minimising the distortions of the plasma wakefield and investigating the beam guiding effects. In the experiment, the acceleration can be controlled by changing the position and duration of the injection (Albert & Thomas 2016; Albert *et al.* 2021). The duration of the accelerating Gaussian laser pulse of $\tau = 10$ fs (the spatial duration equal to $c\tau = 3$ μm) was chosen to fit the width of the plasma structures created by the guiding Bessel–Gauss beam (figure 3). The Gaussian beam radius of $w_0 = 7$ μm was matched to the radius of the first ring of $w_b = 7.5$ μm for the B_1G beam, and $w_b = 11$ μm for the B_2G beam. The laser strength parameter of $a_{0b} = 1.5$ was used based on the Wake-T simulation

https://doi.org/10.1017/S0022377823000247 Published online by Cambridge University Press

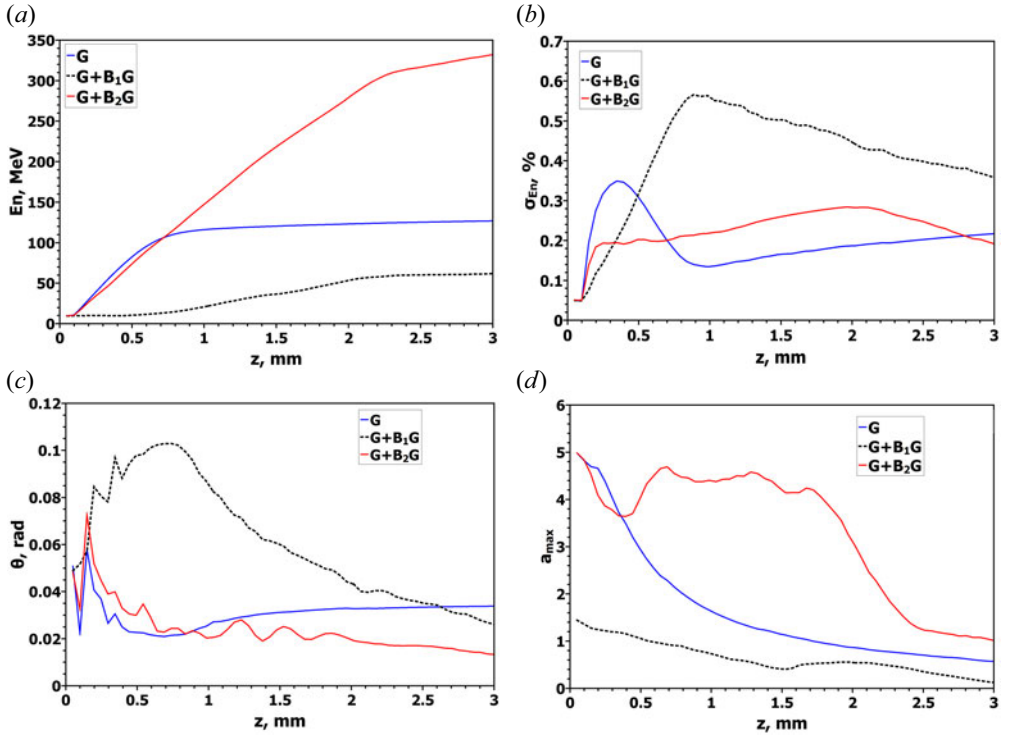

FIGURE 7. Dependence of the (*a*) energy of accelerated electrons, (*b*) energy spread σ_{En}, (*c*) divergence θ_E and (*d*) accelerating pulse amplitude $a_{\max}$ on the acceleration distance for Gaussian (G), Gaussian and B_1G ($G+B_1G$), and Gaussian and B_2G ($G+B_2G$), and laser beams. Parameters of the accelerating Gaussian beam, $a_0 = 5.0$ (for G and $G+B_2G$); $a_0 = 1.5$ (for $G+B_1G$); $\tau = 10$ fs; $w_0 = 7$ μm; and BG beam, $a_{0b} = 1.5$; $\tau_b = 25$ fs. The waist of B_1G is $w_{0b} = 7.5$ μm and the waist of B_2G is $w_{0b} = 11$ μm.

results (figures 1–4). The duration of the guiding Bessel–Gauss beam of $\tau_b = 25$ fs and the initial concentration of electrons in plasma $n_0 = 3 \times 10^{18}$ cm^{-3} were selected based on the maximal charge density in the plasma ring excited by the BG beam (figure 4). The maximum acceleration distance in plasma was $z = 3$ mm, and the divergence of the electron bunch θ_E was defined as an average of $\theta_{Ex,y} = \arctan(u_{x,y}/u_z)$ in the x and y directions, where u_x, u_y and u_z are normalised electron momenta in the directions of x, y and z.

The results of the FBPIC simulation for the Gaussian (G), Gaussian combined with B_1G ($G+B_1G$) and Gaussian combined with B_2G ($G+B_2G$) configurations are shown in figure 7. The highest energy of accelerated electrons with a moderate energy spread and electron-beam divergence were obtained using a Gaussian beam with the laser strength parameter of $a_0 = 5.0$, guided by the B_2G beam with $a_{0b} = 1.5$ ($G+B_2G$ configuration). For that laser strength parameter, the maximum energy of accelerated electrons at $z = 3$ mm reached 332 MeV (figure 7*a*). A saturation in the energy ramp at the 2.3 mm acceleration distance was observed. The energy spread for this configuration was in the range of 20–30 % (figure 7*b*) and the minimum divergence was 27 mrad. (figure 7*c*). The energy spread stabilised after 0.5 mm of acceleration and divergence was improved with the distance.

https://doi.org/10.1017/S0022377823000247 Published online by Cambridge University Press

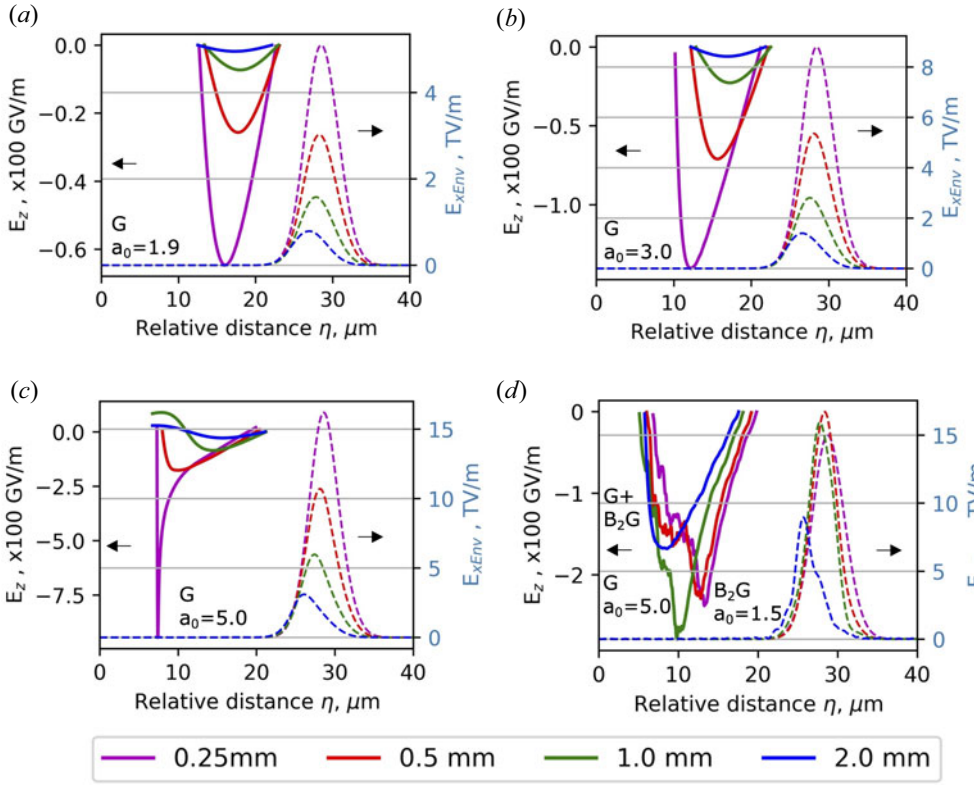

FIGURE 8. Dependence of the longitudinal plasma wake electric field E_z (solid line) and the electric field of laser beam envelope (dotted line) for acceleration distances $z = 0.25$ mm, 0.5 mm, 1 mm, 2 mm of the Gaussian beam with the laser strength parameter (*a*) $a_0 = 1.9$, (*b*) $a_0 = 3.0$, (*c*) $a_0 = 5.0$ and (*d*) the Gaussian beam with $a_0 = 5.0$ guided by the B_2G beam with $a_0 = 1.5$ ($G + B_2G$).

Application only of the Gaussian beam with the same strength parameter $a_0 = 5.0$ was more efficient in LWFA only at short acceleration distances of approximately 0.6 mm, permitting to achieve the electron energy of only 127 MeV, 2.6 times lower than in the $G + B_2G$ configuration. However, the substantial divergence of the focused Gaussian beam after the waist led to a reduction of intensity (a_0). The guided Gaussian beam in the $G + B_2G$ configuration preserved its strength parameter over a longer distance of approximately 2 mm (figure 7*d*).

Guiding the Gaussian beam by the first-order Bessel-Gauss beam ($G + B_1G$) was inefficient because of the interference of the axial longitudinal electric field of the Gaussian and B_1G beam (figure 7*a–c*).

For all values of the parameter a_0 presented in figure 7, the efficient acceleration takes place up to a distance of $z \sim 2$–3 mm. For longer distances, the energy growth slows down significantly or stops growing. Because of the nonlinear phase modulation of the accelerating pulse (nonlinear chirp), the laser beam splits into several beamlets and the amplitude of the central accelerating peak is reduced significantly.

In figures 8–11 and table 1, the results of the FBPIC LWFA simulation and characteristics of the accelerated 1 pC Gaussian electron bunch at the distance of 2 mm,

https://doi.org/10.1017/S0022377823000247 Published online by Cambridge University Press

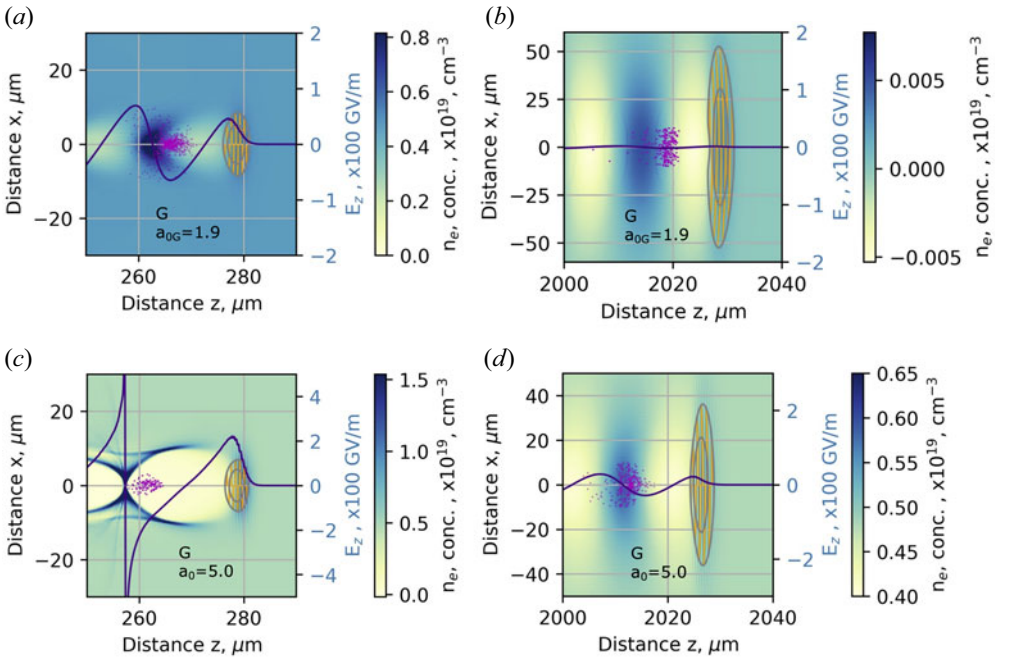

FIGURE 9. Distribution of plasma concentration (colour map) and longitudinal plasma wake electric field E_z (line) formed along a beam axis by the Gaussian beam with the laser strength parameter (*a*,*b*) $a_0 = 1.9$ and (*c*,*d*) $a_0 = 5.0$. Isolines and yellow oscillating lines represent the location and intensity of the electrical field of the laser pulse. The violet cloud is the electron bunch injected behind the laser pulse.

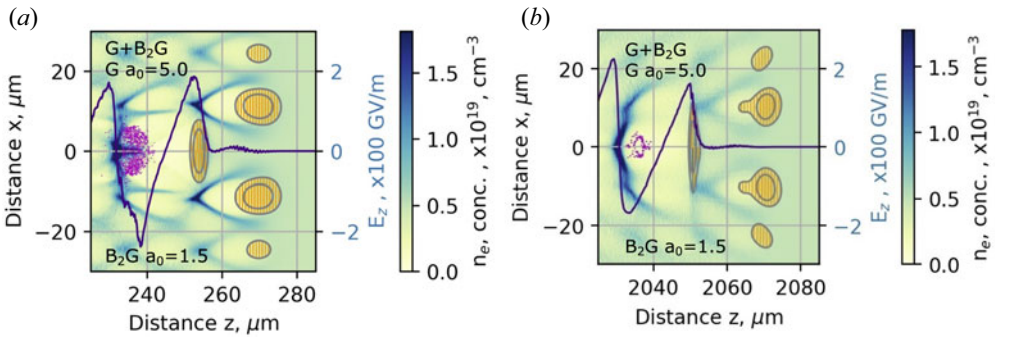

FIGURE 10. (*a*,*b*) Distribution of plasma concentration (colour map) and dependence of longitudinal plasma wake electric field E_z (line) formed behind the Gaussian beam with $a_0 = 5.0$ guided by the B_2G beam with $a_0 = 1.5$. Isolines with yellow oscillating lines represent the location and intensity of the electrical field of the laser pulses. The violet cloud is the electron bunch injected behind the laser pulse.

using the Gaussian beam and the Gaussian beam guided by the B_2G beam, are shown. The laser strength parameters and pulse durations of the beams are also presented in table 1.

The intensity of the Gaussian beam and corresponding plasma wake (GV m^{-1}) fall down rapidly with the propagation distance due to strong diffraction of the Gaussian beam and a short Rayleigh length for a tight, focused Gaussian beam (figure 8*a–c*). The waist

https://doi.org/10.1017/S0022377823000247 Published online by Cambridge University Press

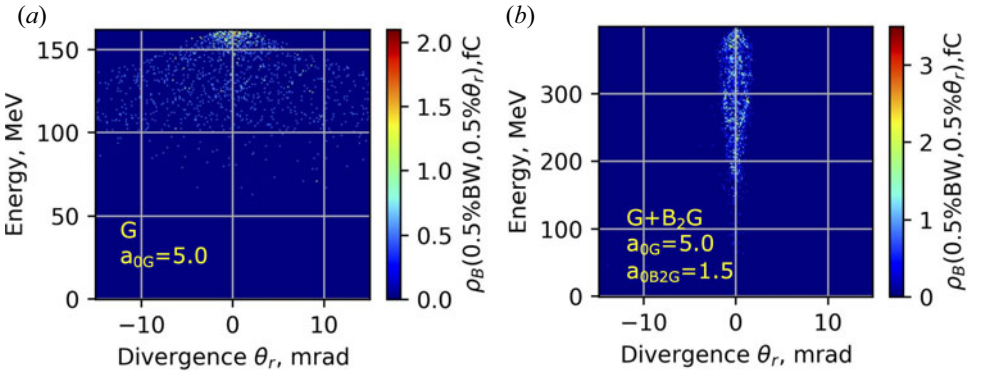

FIGURE 11. Energy and divergence θ_y of electrons accelerated by (*a*) the Gaussian beam with $a_0 = 5.0$ and (*b*) the Gaussian beam with the laser strength parameter $a_0 = 5.0$, guided by the B_2G beam with $a_0 = 1.5$ at the acceleration distance of 2 mm.

radius of the laser beam increases from 7 μm to 50 μm for $a_0 = 1.9$ and to 38 μm for $a_0 = 5.0$ (figure 9*a*,*c*). The diffraction is opposed by nonlinear self-guiding intensive laser beams. With increasing the intensity of the Gaussian beam from $a_0 = 1.9$ to $a_0 = 5.0$, the self-guiding becomes dominant.

The initial value of the laser strength parameter a_0 affects the strength of the longitudinal electrical field E_z, responsible for the acceleration of electrons by the wake. By increasing the acceleration distance from 0.25 mm to 0.5 mm for $a_0 = 1.9$, the electric field of the laser beam envelope drops from 5.0 TV m^{-1} to 3.0 TV m^{-1} and to 0.9 TV m^{-1} at a distance of 2 mm. The longitudinal electric field of the plasma wake drops from 63 GV m^{-1} to 25 GV m^{-1} and to 1 GV m^{-1} at distances of 0.25 mm, 0.5 mm and 2 mm, respectively (figures 8*a* and 9*a*,*b*). The weighted mean energy of the accelerated electron bunch reaches 28 ± 7 MeV and the divergence $\theta_E = 41$ mrad (table 1).

At the distances from 0.25 mm to 0.5 mm for $a_0 = 3.0$, the electric field of the laser beam envelope drops from 8.5 TV m^{-1} to 5.5 TV m^{-1} and to 1.5 TV m^{-1} at 2 mm (figure 8*b*). The longitudinal electric field of the plasma wake drops from 140 GV m^{-1} to 70 GV m^{-1} and to 1.5 GV m^{-1} at the distances of 0.25 mm, 0.5 mm and 2 mm, respectively. The electrons are accelerated up to 53 ± 13 MeV and the divergence $\theta_E = 37$ mrad (table 1).

The wake is shifted back relative to the accelerating laser pulse in the case of a more intense laser pulse, indicating the increase in plasma bubble size. The radius of the plasma bubble increases proportionally to $(a_0)^{1/2}$ allowing a higher acceleration distance of electrons. At the distances from 0.25 mm to 0.5 mm for $a_0 = 5.0$, the electric field of the laser beam envelope drops from 17 TV m^{-1} to 11 TV m^{-1} and to 3 TV m^{-1} at 2 mm (figures 8*c* and 9*c*,*d*). The longitudinal electric field of the plasma wake drops from 800 GV m^{-1} to 180 GV m^{-1} and to 25 GV m^{-1} at distances of 0.25 mm, 0.5 mm and 2 mm, respectively. At the initial acceleration distance from 0.25 mm to 0.5 mm of the nonlinear expansion of the bubble, the minimum of the longitudinal electric field shifts 2.1 times further from the accelerating beam position increasing the dephasing distance of accelerated electrons relative to the $a_0 = 1.9$ case. The electrons are accelerated up to 125 ± 23 MeV, and the divergence $\theta_E = 33$ mrad (figure 11*a* and table 1).

For the $G + B_2G$ configuration, relative to the case in figure 8(*c*), the plasma wake preserves a high accelerating field E_z at the 2.0 mm distance (figure 8*d*). That is clear evidence of the positive guiding effect of the Gaussian beam by the plasma ring produced by the BG beam. The longitudinal electric field of the plasma wake in the central part of the

https://doi.org/10.1017/S0022377823000247 Published online by Cambridge University Press

	Accelerating beam	Guiding beam	a_0 of accelerating beam	a_0 of guiding beam	Pulse duration of accelerating beam, fs	Pulse duration of guiding beam, fs	Weighted average energy of electrons, MeV	Standard deviation of electron energy, MeV	Divergence of electron bunch θ_E, mrad
1.	Gauss	—	1.9	—	10	—	28	7	41
2.	Gauss	—	3.0	—	10	—	53	13	37
3.	Gauss	—	5.0	—	10	—	125	23	33
4.	Gauss	Bessel–Gauss B_2G	5.0	1.5	10	25	283	83	19

TABLE 1. Characteristics of the accelerated 1 pC electron bunch using Gaussian and Bessel–Gauss B_2G beams in plasma with a concentration of 3×10^{18} cm^{-3} at the distance of 2 mm.

B_2G beam is low, of the order of 10 GV m^{-1}, and is formed by the guided Gaussian beam. The electric field of the Gaussian beam envelope remains almost constant at a distance from 0.25 mm to 0.5 mm in the range of 15 TV m^{-1} and drops to 9 TV m^{-1} at 2 mm (figures 8*d* and 10*a*,*b*). The longitudinal electric field of the plasma wake is at the level of 230–270 GV m^{-1} at a distance from 0.25 mm to 0.5 mm and drops to 160 GV m^{-1} at 2 mm. Compared to the Gaussian beam with $a_0 = 5.0$, the absolute values of the laser intensity and longitudinal electric field of the laser beam at the distance of 0.25 mm are almost the same. However, the electric fields of the laser beam and plasma wake at 2 mm are factors of 3.0 and 6.4 higher, respectively. The electrons are accelerated at a higher energy of 283 ± 83 MeV by a factor of 2.3 with the divergence $\theta_E = 19$ mrad (figure 11*b* and table 1).

A Gaussian pulse located behind the B_2G pulse within a ring of high electron concentration (waveguide) (figure 10*a*,*b*) produces a wake with a strong longitudinal electrical field (line) able to accelerate an electron bunch (violet cloud) injected in front of the wake. In addition to electron acceleration, we see a concentration of the bunch closer to the beam propagation axis, which means a reduction in electron bunch divergence. High-energy electron bunches with a moderate energy spread and low divergence could be produced by combining the guiding the Gaussian accelerating pulse with the doughnut-shaped second-order Bessel–Gauss pulse.

5. Conclusions

The Gaussian beam at the acceleration distance of 2 mm in the plasma concentration of $n_0 = 3 \times 10^{18}$ cm^{-3} diffracts substantially, and the waist radius of the laser beam increases from 7 μm to 50 μm for $a_0 = 1.9$ and to 38 μm for $a_0 = 5.0$. The guiding of the Gaussian beam with $a_0 = 5.0$ by the B_2G beam with $a_0 = 1.5$ increases the propagation distance. The electric field of the guided laser beam at the propagation distance of 2 mm is a factor of 3.0 higher relative to the Gaussian beam with $a_0 = 5.0$. The weighted average energy of electrons is a factor of 2.3 higher, and the divergence of electron bunch θ_E is a factor of 1.7 lower compared to the case of the Gaussian beam of the same intensity. At the acceleration distance of 2 mm, the maximum electron energy reaches 283 ± 83 MeV with the divergence $\theta_E = 19$ mrad. Selected acceleration configurations are promising to implement towards VHEE applications. The proposed laser beam guiding technique helps to increase the energy of accelerated electrons enabling the dose deposition at deep-seated tumours.

Acknowledgements

Editor Victor Malka thanks the referees for their advice in evaluating this article.

Declaration of interest

The authors report no conflict of interest.

Funding

The research leading to these results was funded by the Research Council of Lithuania under grant agreement No. S-MIP-21-3.

Author's contributions

V. Girdauskas performed the physical analysis, defined the methodology, carried out the Wake-T and FBPIC simulation, and wrote the original draft. V. Tomkus carried out the physical analysis and FBPIC simulation, and wrote the original draft. M. Abedi-Varaki worked on the physical analysis and FBPIC simulation, and wrote the original draft. G.

https://doi.org/10.1017/S0022377823000247 Published online by Cambridge University Press

Raciukaitis defined the methodology, supervised the research, conceived and defined the aims of the investigation, reviewed and edited the manuscript. All authors reviewed the obtained results and commented on the paper.

Ethics approval

This paper has not been submitted for publication elsewhere. We further certify that proper citations to the previously reported work have been given, and no data/tables/figures have been quoted verbatim from other publications without giving due acknowledgement and without the permission of the author(s).

Data availability

The authors confirm that all of the data and codes used in this study are available from the corresponding author upon reasonable request.

REFERENCES

Albert, F., Couprie, M., Debus, A., Downer, M.C., Faure, J., Flacco, A., Gizzi, L.A., Grismayer, T., Huebl, A. & Joshi, C. 2021 2020 roadmap on plasma accelerators. *New J. Phys*. **23**, 031101.

Albert, F. & Thomas, A.G. 2016 Applications of laser wakefield accelerator-based light sources. *Plasma Phys. Control. Fusion* **58**, 103001.

Andreev, N., Chizhonkov, E., Frolov, A. & Gorbunov, L. 1998 On laser wakefield acceleration in plasma channels. *Nucl. Instrum. Meth. Phy. Res. Sect.* A **410**, 469.

Benedetti, C., Schroeder, C., Geddes, C., Esarey, E. & Leemans, W. 2017 An accurate and efficient laser-envelope solver for the modeling of laser-plasma accelerators. *Plasma Phys. Control. Fusion* **60**, 014002.

Brijesh, P., Thaury, C., Phuoc, K.T., Corde, S., Lambert, G., Malka, V., Mangles, S.P.D., Bloom, M. & Kneip, S. 2012 Tuning the electron energy by controlling the density perturbation position in laser plasma accelerators. *Phys. Plasmas* **19** (6), 063104.

Budriunas, R., Stanislauskas, T., Adamonis, J., Aleknavičius, A., Veitas, G., Gadonas, D., Balickas, S., Michailovas, A. & Varanavičius, A. 2017 53 W average power CEP-stabilized OPCPA system delivering 5.5 TW few cycle pulses at 1 kHz repetition rate. *Opt. Express* **25**, 5797.

Burza, M., Gonoskov, A., Svensson, K., Wojda, F., Persson, A., Hansson, M., Genoud, G., Marklund, M., Wahlström, C.G. & Lundh, O. 2013 Laser wakefield acceleration using wire produced double density ramps. *Phys. Rev. Accel. Beams* **16** (1), 011301.

Cardenas, D.E., Chou, S., Wallin, E., Xu, J., Hofmann, L., Buck, A., Schmid, K., Rivas, D.E., Shen, B., Gonoskov, A., Marklund, M. & Veisz, L. 2020 Electron bunch evolution in laser-wakefield acceleration. *Phys. Rev. Accel. Beams* **23**, 112803.

Chitgar, Z.M., Gibbon, P., Böker, J., Lehrach, A. & Büscher, M. 2020 Electron self-injection threshold for the tandem-pulse laser wakefield accelerator. *Phys. Plasmas* **27**, 023106.

Esarey, E., Schroeder, C. & Leemans, W. 2009 Physics of laser-driven plasma-based electron accelerators. *Rev. Mod. Phys*. **81**, 1229.

Faure, J., Gustas, D., Guénot, D., Vernier, A., Böhle, F., Ouillé, M., Haessler, S., Lopez-Martens, R. & Lifschitz, A. 2018 A review of recent progress on laser-plasma acceleration at kHz repetition rate. *Plasma Phys. Control. Fusion* **61**, 014012.

Fubiani, G., Esarey, E., Schroeder, C.B. & Leemans, W.P. 2004 Beat wave injection of electrons into plasma waves using two interfering laser pulses. *Phys. Rev.* E **70** (1), 016402.

Fuchs, T., Szymanowski, H., Oelfke, U., Glinec, Y., Rechatin, C., Faure, J. & Malka, V. 2009 Treatment planning for laser-accelerated very-high energy electrons. *Phys. Med. Biol*. **54**, 3315.

Golovin, G., Banerjee, B., Chen, S., Powers, N., Liu, C., Yan, W., Zhang, J., Zhang, P., Zhao, B. & Umstadter, D. 2016 Control and optimization of a staged laser-wakefield accelerator. *Nucl. Instrum. Meth. Phys. Res.* A **830**, 375-380.

https://doi.org/10.1017/S0022377823000247 Published online by Cambridge University Press

GONSALVES, A.J., NAKAMURA, K., LIN, C., PANASENKO, D., SHIRAISHI, S., SOKOLLIK, T., BENEDETTI, C., SCHROEDER, C.B., GEDDES, C.G.R.R., VAN TILBORG, J., OSTERHOFF, J., ESAREY, E., TOTH, C. & LEEMANS, W.P. 2011 Tunable laser plasma accelerator based on longitudinal density tailoring. *Nat. Phys*. **7** (11), 862-866.

GONSALVES, A., NAKAMURA, K., DANIELS, J., BENEDETTI, C., PIERONEK, C., DE RAADT, T., STEINKE, S., BIN, J., BULANOV, S. & VAN TILBORG, J. 2019 Petawatt laser guiding and electron beam acceleration to 8 GeV in a laser-heated capillary discharge waveguide. *Phys. Rev. Lett*. **122**, 084801.

HANSSON, M., AURAND, B., DAVOINE, X., EKERFELT, H., SVENSSON, K., PERSSON, A., WAHLSTRÖM, C.G. & LUNDH, O. 2015 Down-ramp injection and independently controlled acceleration of electrons in a tailored laser wakefield accelerator. *Phys. Rev. Accel. Beams* **18** (7), 071303.

HAO, Z., ZHANG, J., LI, Y., LU, X., YUAN, X., ZHENG, Z., WANG, Z., LING, W. & WEI, Z. 2005 Prolongation of the fluorescence lifetime of plasma channels in air induced by femtosecond laser pulses. *Appl. Phys.* B **80**, 627.

HIDDING, B., ASSMANN, R., BUSSMANN, M., CAMPBELL, D., CHANG, Y.-Y., CORDE, S., CABADAG, J.C., DEBUS, A., DÖPP, A., GILLJOHANN, M., *et al.* 2023 Progress in hybrid plasma wakefield acceleration. *Photonics* **10**, 99.

KOKUREWICZ, K., BRUNETTI, E., WELSH, G., WIGGINS, S., BOYD, M., SORENSEN, A., CHALMERS, A., SCHETTINO, G., SUBIEL, A. & DESROSIERS, C. 2019 Focused very high-energy electron beams as a novel radiotherapy modality for producing high-dose volumetric elements. *Sci. Rep*. **9**, 10837.

LEEMANS, W., GONSALVES, A., MAO, H.-S., NAKAMURA, K., BENEDETTI, C., SCHROEDER, C., TÓTH, C., DANIELS, J., MITTELBERGER, D. & BULANOV, S. 2014 Multi-GeV electron beams from capillary-discharge-guided Subpetawatt laser pulses in the self-trapping regime. *Phys. Rev. Lett*. **113**, 245002.

LEHE, R., KIRCHEN, M., ANDRIYASH, I.A., GODFREY, B.B. & VAY, J.-L. 2016 A spectral, quasi-cylindrical and dispersion-free particle-in-cell algorithm. *Comput. Phys. Commun*. **203**, 66-82.

LEMOS, N., CARDOSO, L., GEADA, J., FIGUEIRA, G., ALBERT, F. & DIAS, J. 2018 Guiding of laser pulses in plasma waveguides created by linearly-polarized femtosecond laser pulses. *Sci. Rep*. **8**, 3165.

LU, X., CHEN, S.-Y., MA, J.-L., HOU, L., LIAO, G.-Q., WANG, J.-G., HAN, Y.-J., LIU, X.-L., TENG, H. & HAN, H.-N. 2015 Quasi-steady-state air plasma channel produced by a femtosecond laser pulse sequence. *Sci. Rep*. **5**, 15515.

MALKA, V., FAURE, J., GAUDUEL, Y.A., LEFEBVRE, E., ROUSSE, A. & PHUOC, K.T. 2008 Principles and applications of compact laser–plasma accelerators. *Nat. Phys*. **4**, 447-453.

MASSIMO, F., LIFSCHITZ, A.F., THAURY, C. & MALKA, V. 2017 Numerical studies of density transition injection in laser wakefield acceleration. *Plasma Phys. Control. Fusion* **59** (8), 085004.

MILCHBERG, H., KIM, K., KUMARAPPAN, V., LAYER, B. & SHENG, H. 2006 Clustered gases as a medium for efficient plasma waveguide generation. *Phil. Trans. R. Soc.* A*: Math. Phys. Engng Sci.* **364**, 647.

MIRZAIE, M., LI, S., ZENG, M., HAFZ, N.A.M., CHEN, M., LI, G.Y., ZHU, Q.J., LIAO, H., SOKOLLIK, T., LIU, F., MA, Y.Y., CHEN, L.M., SHENG, Z.M. & ZHANG, J. 2015 Demonstration of self-truncated ionization injection for GeV electron beams. *Sci. Rep*. **5**, 14659.

MOHAMED, W.T., CHEN, G., KIM, J., TAO, G.X., AHN, J. & KIM, D.E. 2011 Controlling the length of plasma waveguide up to 5 mm, produced by femtosecond laser pulses in atomic clustered gas. *Opt. Exp*. **19**, 15919.

OSTERHOFF, J., POPP, A., MAJOR, Z., MARX, B., ROWLANDS-REES, T., FUCHS, M., GEISSLER, M., HÖRLEIN, R., HIDDING, B. & BECKER, S. 2008 Generation of stable, low-divergence electron beams by laser-wakefield acceleration in a steady-state-flow gas cell. *Phys. Rev. Lett*. **101**, 085002.

PALASTRO, J., SHAW, J., FRANKE, P., RAMSEY, D., SIMPSON, T. & FROULA, D. 2020 Dephasingless laser wakefield acceleration. *Phys. Rev. Lett*. **124**, 134802.

POUSA, A., AßMANN, R. & DE LA OSSA, A. 2019 Wake-T: a fast particle tracking code for plasma-based accelerators. *J. Phys.: Conf. Ser*. **1350**, 012056.

PUKHOV, A. 2015 Particle-in-cell codes for plasma-based particle acceleration. Preprint, arXiv:1510.01071.

ROVIGE, L., HUIJTS, J., ANDRIYASH, I., VERNIER, A., TOMKUS, V., GIRDAUSKAS, V., RACIUKAITIS, G., DUDUTIS, J., STANKEVIC, V., GECYS, P., OUILLE, M., CHENG, Z., LOPEZ-MARTENS, R. & FAURE, J. 2020 Demonstration of stable long-term operation of a kilohertz laser-plasma accelerator. *Phys. Rev. Accel. Beams* **23**, 093401.

SHALLOO, R., ARRAN, C., CORNER, L., HOLLOWAY, J., JONNERBY, J., WALCZAK, R., MILCHBERG, H. & HOOKER, S. 2018 Hydrodynamic optical-field-ionized plasma channels. *Phys. Rev.* E **97**, 053203.

SMARTSEV, S., CAIZERGUES, C., OUBRERIE, K., GAUTIER, J., GODDET, J.-P., TAFZI, A., PHUOC, K.T., MALKA, V. & THAURY, C. 2019 Axiparabola: a long-focal-depth, high-resolution mirror for broadband high-intensity lasers. *Opt. Lett*. **44**, 3414.

SUBIEL, A., MOSKVIN, V., WELSH, G.H., CIPICCIA, S., REBOREDO, D., DESROSIERS, C. & JAROSZYNSKI, D.A. 2017 Challenges of dosimetry of ultra-short pulsed very high energy electron beams. *Phys. Medica* **42**, 327.

TANG, R.-A., YIN, L.-R., HONG, X.-R., GAO, J.-M., CHENG, L.-H. & XUE, J.-K. 2020 Propagation dynamics of an azimuthally polarized Bessel–Gauss laser beam in a parabolic plasma channel. *Phys. Plasmas* **27**, 113103.

TOMASSINI, P., DE NICOLA, S., LABATE, L., LONDRILLO, P., FEDELE, R., TERZANI, D., NGUYEN, F., VANTAGGIATO, G. & GIZZI, L. 2018 High-quality GeV-scale electron bunches with the resonant multi-pulse ionization injection. *Nucl. Instrum. Meth. Phys. Res.* A **909**, 1.

TZORTZAKIS, S., PRADE, B., FRANCO, M. & MYSYROWICZ, A. 2000 Time-evolution of the plasma channel at the trail of a self-guided IR femtosecond laser pulse in air. *Opt. Commun*. **181**, 123.

VIEIRA, J. & MENDONÇA, J. 2014 Nonlinear laser driven donut wakefields for positron and electron acceleration. *Phys. Rev. Lett*. **112**, 215001.

ZHANG, G.-B., CHEN, M., LUO, J., ZENG, M., YUAN, T., YU, J.-Y., MA, Y.-Y., YU, T.-P., YU, L.-L. & WENG, S.-M. 2016 Acceleration of on-axis and ring-shaped electron beams in wakefields driven by Laguerre-Gaussian pulses. *J. Appl. Phys*. **119**, 103101.